

Tuning the bond order wave (BOW) phase of half-filled extended Hubbard models

Manoranjan Kumar¹, S. Ramasesha¹, Z.G. Soos²

¹*Solid State and Structural Chemistry Unit, Indian Institute of Science, Bangalore 5600 12, India,*

²*Department of Chemistry, Princeton University, Princeton, N.J. 08544, USA*

(Dated: February 6, 2020)

Theoretical and computational studies of the quantum phase diagram of the one-dimensional half-filled extended Hubbard model (EHM) indicate a narrow bond order wave (BOW) phase with finite magnetic gap E_m for on-site repulsion $U < U^*$, the critical point, and nearest neighbor interaction $V_c \approx U/2$ near the boundary of the charge density wave (CDW) phase. Potentials with more extended interactions that retain the EHM symmetry are shown to have a less cooperative CDW transition with higher U^* and wider BOW phase. Density matrix renormalization group (DMRG) is used to obtain E_m directly as the singlet-triplet gap, with finite E_m marking the BOW boundary $V_s(U)$. The BOW/CDW boundary $V_c(U)$ is obtained from exact finite-size calculations that are consistent with previous EHM determinations. The kinetic energy or bond order provides a convenient new estimate of U^* based on a metallic point at $V_c(U)$ for $U < U^*$. Tuning the BOW phase of half-filled Hubbard models with different intersite potentials indicates a ground state with large charge fluctuations and magnetic frustration. The possibility of physical realizations of a BOW phase is raised for Coulomb interactions.

PACS 71.10.Fd, 71.30.+h, 71.45.Lr

PACS numbers:

I. INTRODUCTION

The quantum phase diagram of the half-filled extended Hubbard model (EHM) in one dimension (1D) illustrates competition among on-site repulsion $U > 0$, nearest-neighbor interaction V and electron transfer t . Large U gives a ground state (gs) with one electron per site while large $V > 0$ leads alternately to empty and doubly occupied sites. The gs phase diagram and its critical point U^* have evolved since Hirsch's original study [1] of the boundary between a spin density wave (SDW) at large U and a charge density wave (CDW) at large V . Nakamura [2] first proposed a bond order wave (BOW) phase between the SDW and CDW up to a critical $U = U^*$. The schematic quantum phase diagram in Fig.1 follows Sengupta *et al.* [3] and recent works by Zhang [4] and by Glocke *et al.* [5]. The CDW boundary that we denote as $V_c(U)$ has readily been found numerically. The value of U^* and the SDW boundary at $V_s(U) < V_c$ are more challenging. The BOW phase is much narrower than sketched and lies between [4, 5] V_s and V_c for $U < U^* \approx 7t$. It is insulating and has a finite magnetic gap, E_m , that is expected to be very small because $V_s(U)$ is a Kosterlitz-Thouless transition [2]. Finite E_m implies *electronic* dimerization leading to long-range order at 0 K.

Multiple theoretical methods have been applied to the quantum phase diagram at 0 K. They include field-theoretical analysis of continuum models [2, 6], weak-coupling expansions [7], Monte Carlo simulations [1, 3], density matrix normalization group (DMRG) methods [4, 8, 9] and the transfer matrix renormalization group (TMRG) [5], in addition to exact diagonalization [10] of finite systems and perturbation expansions about the

weak and strong coupling limits. The BOW phase for weak coupling (small U, V) has recently been demonstrated [9] for the EHM by functional renormalization group.

In this paper, we study the 0 K phase diagram of half-filled extended 1D Hubbard models with intersite interactions V_m that are not restricted to $V_1 \equiv V$. Any spin-independent V_m retains [11] the translational, spin, and electron-hole symmetry of the EHM. Suitable potentials have electrostatic energy $-V\alpha_M/2$ per site, with Madelung constants $\alpha_M = 2$ for EHM, $2\ln 2$ for point charges, etc. The CDW transition at large V becomes less cooperative for $1 < \alpha_M < 2$, thereby extending the BOW phase to larger critical U^* and increasing the width $V_c(U) - V_s(U)$. We introduce a convenient new way to find U^* and $V_c(U)$ based on the kinetic energy or bond order $p(U, V)$, which is maximized at a metallic point where the large U and V are balanced. The threshold of the BOW phase for $U < U^*$ is obtained by DMRG calculation of the magnetic gap E_m . Within the DMRG accuracy, finite E_m at $V_s(U)$ below $V_c(U)$ sets a lower bound on the onset of the BOW phase.

Competing interactions are widely invoked for materials whose gs depends sensitively on small changes [12]. The EHM literature deals with many-body techniques and ideas without regard to possible physical realization. Coulomb interaction between point charges is more physical. As in metal-insulator or Mott transitions, however, the assumption of purely *electronic* transitions is inherently an approximation. The SDW is unstable to a Peierls transition leading to dimerization for any harmonic lattice. Lattice dimerization corresponds to well-understood BOW phases that are realized in quasi-1D systems such as organic ion-radical salts [13] and charge-transfer (CT) salts [14] or conjugated polymers [15, 16].

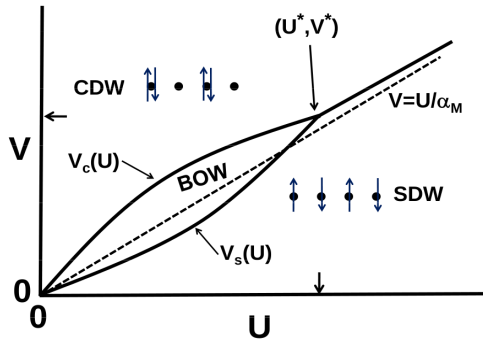


FIG. 1: Schematic quantum phase diagram of half-filled extended Hubbard models with on-site $U > 0$, nearest-neighbor V and 1D potential with Madelung constant α_M . The SDW/CDW transition line $V_c(U)$ is first order for $U > U^*$, the critical point, and second order for $U < U^*$. The BOW phase between $V_s(U)$ and $V_c(U)$ is a Mott insulator with a metallic point at V_c and a finite magnetic gap, E_m , that opens at V_s .

Such systems have intermediate correlation $(U - V) > 2t$. The present study is restricted to a rigid 1D lattice with purely electronic instabilities. Possible physical realizations are mentioned in the Discussion.

Previous EHM studies [1, 2, 3, 4, 5, 6, 7, 8, 9, 10] have focused on gs correlation functions for charge, spin or bond order as well as various susceptibilities. Our DMRG calculations target instead E_m directly as the singlet-triplet gap, E_{ST} , between the lowest triplet state and singlet gs. We also present exact finite-size results that have been used to model the neutral-ionic transition of CT salts [17]. Contributions due to t are particularly important at $V_c(U)$. The line $V_c(U)$ up to U^* that marks a continuous transition is a metallic point with special properties according to the Berry-phase formulation of polarization [18, 19]. The motivations of the present work are to increase the range and width of the BOW phase by changing the intersite potential. In addition to the computational advantages of a wide BOW phase, control of the width is a step towards understanding a poorly characterized gs. On the SDW side, we refer to previous mappings [20, 21] of Hubbard models onto effective spin Hamiltonians with frustration [22]. Different perspectives on the 0 K phase diagram of EHMs are consistent with other EHM results that also serve as checks for long range potentials.

The paper is organized as follows. Extended Hubbard models with spin-independent intersite potentials are defined in Section II along with bond orders, phase boundaries and the metallic point. DMRG calculations for the magnetic gap E_m and exact finite-size results for $V_c(U)$ and U^* are presented in Section III and compared to prior EHM results. The range and width of the BOW in-

crease for less cooperative potentials. Section IV briefly discusses possible realizations of BOW systems and interpretations in terms of charge fluctuations and magnetic frustration.

II. PHASE BOUNDARIES OF HUBBARD MODELS WITH EXTENDED INTERACTIONS

We consider a half-filled 1D Hubbard model with periodic boundary conditions (PBC), interaction potential V_m between m^{th} neighbors, on-site repulsion $U > 0$ and nearest-neighbor transfer t ,

$$\hat{H} = -t \sum_{p,\sigma} (\hat{a}_{p\sigma}^\dagger \hat{a}_{p+1\sigma} + h.c.) + \sum_p \frac{U}{2} \hat{n}_p (\hat{n}_p - 1) + \sum_p \sum_{m>0} V_m (\hat{n}_p - 1) (\hat{n}_{p+m} - 1) \quad (1)$$

The number operators \hat{n}_p have eigenvalues $n_p = 0, 1$ or 2 . As written, the interaction energy is zero when $n_p = 1$ at all sites, at density $\rho = 1$. The Hellmann-Feynman theorem gives the weight or density of doubly occupied sites in the gs as

$$\rho_2(U, V) = (2N)^{-1} \sum_p \langle \hat{n}_p (\hat{n}_p - 1) \rangle = \frac{1}{N} \frac{\partial E_0}{\partial U} \quad (2)$$

where E_0 is the exact gs energy. Stoichiometry relates the densities of cationic sites (holes) with $n_p = 0$ and anionic sites (electrons) with $n_p = 2$ as $\rho_0 = \rho_2 = (1 - \rho)/2$. The choice of V_m is open, subject to the constraint of spin-independent interactions with $V \equiv V_1$. We note that

$$V_m(a) = V \frac{(a+1)}{(a+m)} \quad (3)$$

corresponds to the EHM in the limit $a \rightarrow -1$, to a point charge model (PCM) at $a = 0$, and slower decrease for $a > 0$ that mimic molecular sites in a delocalized charge model (DCM). The electrostatic energy per two sites of the CDW with holes on one sublattice and electrons on the other is

$$E_M(a) = 2 \sum_{m>0} (-1)^m V_m(a) \equiv -V \alpha_M(a) \quad (4)$$

The Madelung constant α_M defined in Eq. 4 is easily evaluated analytically for integer values of a .

In the strong-coupling or localized limit ($t = 0$), the SDW/CDW boundary is simply $U = V \alpha_M$, the dashed line in Fig. 1. The gs for large U has $n_p = 1$ at all sites and two-fold spin degeneracy at each site, while the gs at large V is a doubly degenerate CDW. The curvature [23] of $V_m(a)$ ensures that the gs at $t = 0$ is either the SDW or the CDW. In this limit, we have $dV/dU \rightarrow 1/\alpha_M$ and the density ρ_2 jumps from 0 to $1/2$ at $V_c = U/\alpha_M$ on increasing V at constant U . For finite t , the discontinuity

of ρ_2 at $V_c(U)$ decreases and vanishes at $V^* = V_c(U^*)$ when the transition becomes continuous.

Translational symmetry leads to uniform bond order $p(U, V)$, proportional to the gs expectation value of the kinetic energy part of Eq. 1,

$$p(U, V) = \frac{1}{2N} \sum_{p\sigma} \langle (\hat{a}_{p\sigma}^\dagger \hat{a}_{p+1\sigma} + h.c.) \rangle = -\frac{1}{2N} \frac{\partial E_0}{\partial t} \quad (5)$$

$U = V = 0$ is a metallic point with $p_0 = 2/\pi$ for a half-filled 1D band. The bond order of extended Hubbard models has a maximum at $V_c(U)$. A first-order transition for $U > U^*$ is indicated by discontinuous $p(U, V)$ at $V_c(U)$, while a second-order transition for $U < U^*$ has continuous $p(U, V)$ that develops a kink at $p(U^*, V^*)$.

The modern theory of polarization in solids grew out of the necessity of incorporating PBC for practical supercell calculations [18]. Subsequent generalizations of the theory and its relation to Berry phases have diverse applications, including how to distinguish between metals and insulators [19]. The theory is applicable to correlated models with neutral-ionic transitions [24] or to models in Eq. 1 with any potential V_m . For EHMs, we require the exact gs of 1D supercells with N sites and PBC to compute the expectation value [24]

$$Z_N(U, V) = \langle \exp(\frac{2\pi i \hat{M}}{N}) \rangle \quad (6)$$

\hat{M} is the conventional dipole operator for unit charge and unit spacing in 1D

$$\hat{M} = \sum_p p(\hat{n}_p - 1). \quad (7)$$

Extended models in Eq. 1 have inversion symmetry at each site and at the center of each bond. The corresponding symmetries for finite N are reflections through sites or through bonds. Either symmetry ensures that Z_N is real in general for EHMs and reduces Z_N to the twist operator [18] with $\cos(2\pi \hat{M}/N)$ instead of the exponential in Eq. 6. Quite generally, we have $Z_N \approx 1$ when the gs consists largely of sites with $n_p = 1$ in the SDW phase and $Z_N \approx -1$ when the gs is a CDW with $n_p = 2$ on one sublattice, $n_p = 0$ on the other. Hence the sign of Z_N changes as V increased at constant U . The point $Z_N(U, V_c) = 0$ for $U < U^*$ corresponds to a metal [19] that separates two insulating phases.

III. MAGNETIC GAP AND METALLIC POINT

In this section we study the gs of \hat{H} in Eq. 1 for potentials $V_m(a)$ using density matrix renormalization group (DMRG) and exact finite-size calculations. Since \hat{H} conserves total spin, E_m is the singlet-triplet gap between the singlet gs and the lowest triplet state. We take $t = 1$ as the unit of energy and find E_m as the difference between the lowest energy states with total $M_S = 1$ and 0.

DMRG with PBC is found to be very accurate when the ring is expanded from the middle by two sites at each step. Earlier DMRG introduced one site in the middle and another at the end of the block spins [25]. This had the disadvantage of adding a bond between a new site and the first site, whose operators have already been renormalized many times. The accurate DMRG-PBC procedure treats the ring as two chains that are joined at the ends.

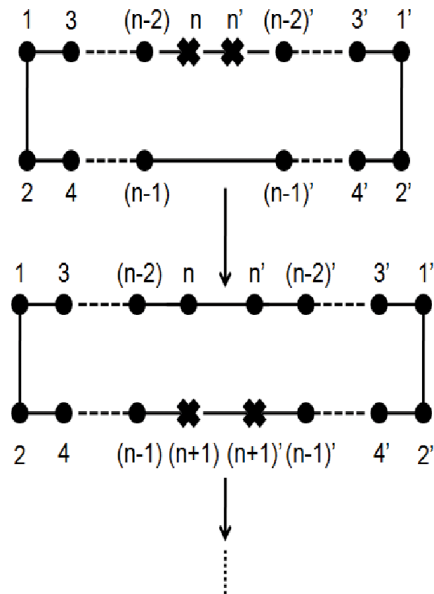


FIG. 2: Infinite DMRG procedure for a system with periodic boundary condition. Sites on left and right blocks are numbered as unprimed and primed integers respectively. Old sites are shown as filled circles and sites added at the DMRG steps are represented by crosses.

At each DMRG step, two sites are added, alternately, in the middle of one chain. The schematic diagrams are shown (see Fig. 2). The new transfer terms at $2n$ system size are (n, n') , $[(n-1), (n-1)']$, $[(n, (n-2)']$ and $[(n-2), n']$. The electron-electron interactions are diagonal and hence are known to be accurate even when interacting sites are separated by several renormalization steps. The procedure introduces explicit transfers between sites whose operators have been renormalized only twice. We have carried out finite DMRG calculation for every $4n$ system size for increased accuracy.

To calculate E_m , we retain $m = 150$ dominant density matrix eigenvectors for states in Eq. 1 with either total $M_S = 0$ or 1. Each DMRG step gives $E_m(N)$ with N increasing by two. We have performed DMRG calculations with finite ring size $N = 4n$ and find that one finite DMRG sweep is sufficient for good convergence of the energy. Fig. 3 shows representative $E_m(N)$ vs. $1/N$ results up to $N > 50$ for the EHM ($a = 1$) and PCM ($a = 0$) at $U = 4$ for several values of V . Good $1/N$ dependencies are found and yield the extrapolated E_m in Fig. 3. Other U and potentials $V_m(a)$ show similar $1/N$ behav-

ior for small E_m when $V < V_c(U)$, while $V > V_c$ results in large $E_m \approx 1$ that increase rather than decrease with N . We estimate the accuracy of extrapolated E_m 's by comparison with $E_m = 0$ in the Hubbard model ($V = 0$) or in the SDW phase ($V < V_s(U)$). The extrapolated E_m/t are ≈ 0.005 . Accordingly, we have assumed that the spin gap is finite when $E_m/t > 0.01$. We verified that E_m does not depend significantly on the choice of m for $m \geq 130$. Much larger m leads to computational difficulties since the sparseness of the Hamiltonian matrix is significantly reduced. The $1/N$ dependence of $E_m(N)$ is monitored to find N after which the extrapolated value changed by less than 0.001, and another iteration was then performed.

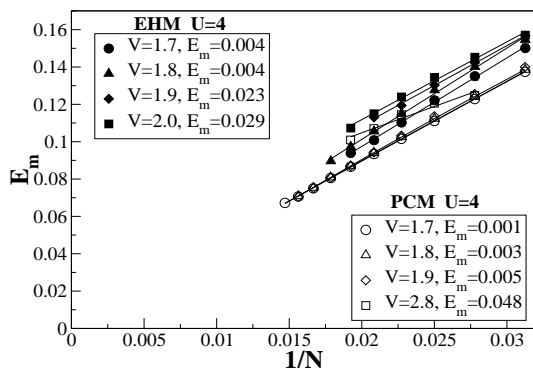


FIG. 3: Singlet-triplet gap, E_m , of Eq. 1 with N sites and periodic boundary conditions vs. $1/N$ for EHM with $a = -1$ in Eq. 3 and PCM with $a = 0$. Extrapolation is between $N = 28$ and $N > 50$. The insets specify U , V and the extrapolated $|E_m| < 0.01$.

To show the threshold $V_s(U)$ for opening a magnetic gap, we plot E_m in Fig. 4 at $U = 4$ for EHM and PCM ($a = 0$ in Eq. 3). Dashed lines V_s at $E_m = 0.01$ indicate the SDW/BOW boundary within our DMRG accuracy. The magnetic gap opens more slowly for PCM than for EHM and more slowly still for delocalized charges (DCM, $a = 1$, not shown). Dashed lines at V_c indicate the BOW/CDW boundary that is found below. Similar DMRG evaluation of $E_m = 0.01$ for other U and $V_m(a)$ combinations yield the $V_s(U)$ entries in Table 1. We find the EHM gap to open at $V_s = 1.86$ for $U = 4$. In this case, direct evaluation of E_m is close to early estimates [2, 3] of the opening of the magnetic gap, while recent calculations [4, 5] give $V_s \approx 2.02$. The DMRG result in ref. 4 is based on a broad peak at V_s that would presumably sharpen in larger systems. The TMRG result in ref. 5 is a thermodynamic method at finite temperature that nevertheless gives estimates for 0 K properties on extrapolation. We find a substantial $E_m = 0.036$ for the EHM at $U = 4$ and $V = 2$.

The CDW boundary at $V_c(U)$ has been found by diverse methods, as tabulated in ref. 8 for the EHM at

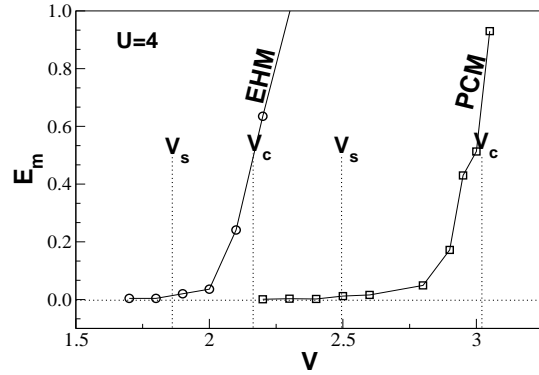


FIG. 4: Extrapolated singlet-triplet gaps, E_m , vs. V for EHM and PCM at $U = 4$. The vertical dashed lines V_s marks $E_m = 0.01$, the DMRG uncertainty (see text). The vertical dashed lines V_c mark the metallic point $V_c(4)$ discussed in the text.

$U = 4$; the range is $2.10 < V_c(4) < 2.16$. Here we evaluate $V_c(U)$ for finite systems of N sites and PBC in Eq. 1. Exact correlated states of Hubbard-type models, currently up to $N = 16$, are found using a many-electron basis of valence bond diagrams [26]. As discussed in connection with the neutral-ionic transition in donor-acceptor stacks [17], the gs has a symmetry crossover at $V_c(U, N)$ for $N = 4n$ that depends weakly ($\approx 1/N^2$) on N . The bottom panel of Fig. 5 shows the $U = 4$ crossover of the EHM from a singlet gs with even electron-hole symmetry that transforms as $k = \pi$ for $V < V_c(4, 16) = 2.10$ and as $k = 0$ for $V > V_c$. Moreover, we find $\rho_2(U, V) = 1/4$ and $Z_N(U, V) = 0$ for the $k = 0$ singlet at almost exactly $V = V_c(U, N)$ for $U < U^*$. The EHM crossovers at $U = 4$ for $N = 8, 12$, and 16 extrapolate to $V_c(4) = 2.16 \pm 0.01$, the entry in Table 1. Tighter extrapolation is possible using $N = 4n + 2$ rings with antiperiodic boundary conditions [17], but this was not pursued. Finite-size corrections to V_c are even smaller for EHM at $U = 6$ or 10 . They are somewhat larger for PCM, whose $V_c(U)$ entries in Table 1 have estimated uncertainties of ± 0.02 , and larger still for DCM with $V_c(U)$ uncertainties of ± 0.03 .

The boundaries of the BOW phase for several potentials are listed in Table 1. The SDW/BOW threshold $V_s(U)$ corresponds to $E_m = 0.01$. The BOW/CDW boundary $V_c(U)$ is the extrapolated gs crossover, the metallic point for $U < U^*$. The $U = 4, 6$ and 10 entries clearly show increasing $V_c - V_s$ as α_M decreases and the CDW transition becomes less cooperative. The demonstration of a BOW phase is then less demanding than for the EHM, where conflicting $U = 4$ results [3, 4, 5] were debated until recently. In particular, substantial $E_m/t > 0.2$ are achieved for the PCM and DCM at $V < V_c(4)$. Such gaps are robust numerically and easily exceed $k_B T$ in organic π -radical stacks [13] with $t \approx 0.1 - 0.3 eV$. It has been fully appreciated that an

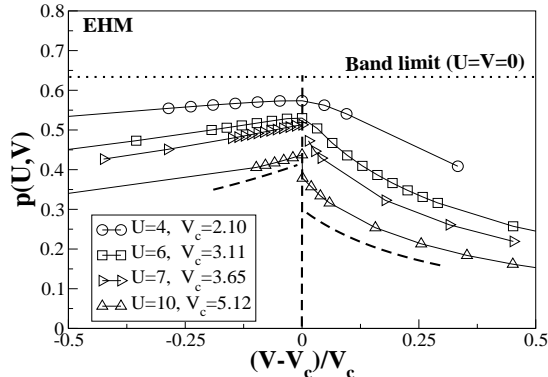


FIG. 5: Lowest energy singlets, both with e-h symmetry $+1$, for EHM with $U = 4$ and 16 sites. Open squares, $B_u(k = \pi)$; stars, $A_g(k = 0)$. Panels (a) and (b) are Z in Eq. 6 and ρ_2 in Eq. 2. Panel (c) shows the gs crossover, with $E = 0$ for B_u and ΔE for A_g .

exponentially small E_m poses numerical difficulties. The present results are upper bounds for V_s at finite E_m . The BOW phase narrows at $U = 6$ and is absent for the EHM at $U = 10$. Our interpretation, continued in the Discussion, is that a BOW gs requires large t in Eq. 1 and strong charge fluctuations.

TABLE I: BOW phase between $V_c - V_s$ for three potentials, EHM, PCM and DCM, with $a = -1, 0$, and 1 in Eq. 3, at $U = 4, 6$ and 10 . The threshold $V_s(U)$ has magnetic gap $E_m = 0.01$, while $V_c(U)$ is the CDW boundary. The critical point U^* has $V_s = V_c$ and no BOW phase. The Madelung constant, α_M in Eq. 4, decreases for less cooperative transitions

Models	EHM ($a = -1$)		PCM ($a = 0$)		DCM ($a = 1$)	
	V_s	V_c	V_s	V_c	V_s	V_c
$U = 4$	1.86	2.16	2.50	3.02	2.70	3.35
$U = 6$	3.06	3.10	4.26	4.45	4.63	5.03
$U = 10$	5.11	5.12	7.33	7.42	8.23	8.35
U^*	6.7 ± 0.2		10.6 ± 0.3		13.3 ± 0.5	
α_M	2		$2\ln 2$		$4(1 - \ln 2)$	

We turn next to the critical point U^* , whose evaluation has been challenging. The most recent EHM values are $U^* = 6.7 \pm 0.2$ (ref. 5) or 7.2 (ref. 4), almost twice the first estimates from Monte Carlo simulations. We obtain U^* from the kinetic energy at $V_c(U)$ as follows. The bond order $p(U, V)$ in Eq. 5 is a continuous function of V for $U < U^*$ with a maximum at the metallic point $V_c(U)$. The peak narrows with increasing U . A kink develops at $p(U^*, V^*)$ and $p(U, V)$ is discontinuous for $U > U^*$, where the transition is first order and there is neither a BOW phase nor a metallic point. Large U generates a discontinuity in $p(U, V)$ at $V_c(U)$, with less kinetic energy on the CDW side. Second-order perturbation theory for the energy and Eq. 5 provide a simple expression for the

bond order,

$$p^{(2)}(U, V) = \frac{4t\ln 2}{V_c(\alpha_M - 1) + (V_c - V)}, V < V_c \quad (8)$$

$$p^{(2)}(U, V) = \frac{2t}{V_c(\alpha_M - 1) + (V - V_c)(2\alpha_M - 1)}, V > V_c.$$

Although $U \approx 10$ is not in the big- U limit, Eq. 8 rationalizes direct evaluation of $p(U, V)$ and the onset of a discontinuity at $U = V_c\alpha_M$.

Figures 6 and 7 show $p(U, V)$ of $N = 16$ rings for the EHM and PCM, respectively, for the indicated values of U . The band limit ($U = V = 0$) of the extended system is $p_0 = 2/\pi$; the analytical result for $N = 16$ is 1.3% less

$$p_0(16) = \frac{1 + \sqrt{2} + 2(\cos \phi + \sin \phi)}{8} = 0.62842 \quad (9)$$

where $\phi = 2\pi/16$. The band limit is the dashed horizontal line when plotted against $(V - V_c)/V_c$. In interacting models of Eq. 1, $p(U, V)$ has a broad maximum at V_c that is less than p_0 and that sharpens with increasing U for either potential. The kinetic energy at the metallic point decreases slowly. Careful examination of the $U = 6$ curve in Fig. 7 shows that for $N = 16$, $p(6, V_c)$ is slightly larger for the gs on the CDW side. The $U = 4$ and 6 curves in Fig. 6 show the same effect for the EHM. We used additional values of U as well as $N = 12$ and 16 results to estimate U^* as the onset of discontinuous $p(U, V)$. The U^* entries in Table 1 increase as expected with decreasing α_M . $U^* = 6.7$ for EHM agrees with the two recent calculations [4, 5]. The dashed line in Fig. 6 for EHM is $p^{(2)}$ in Eq. 8 with $V_c = 5.12$, scaled by a factor of 0.80; the dashed line in Fig. 7 for PCM is $p^{(2)}$ with $V_c = 11.65$ and a scale factor of 0.75. The perturbation result captures most of the $p(U, V)$ discontinuity.

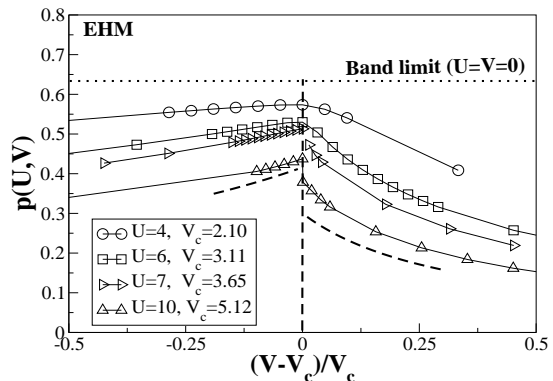


FIG. 6: Bond order, $p(U, V)$ in Eq. 5, vs. $(V - V_c)/V_c$ for EHM with $U = 4, 6, 7$ and 10 . The dotted line is the band limit, $p_0 = 2/\pi$; the dashed line is the strong-coupling limit, Eq. 8 with $V_c = 5.1$, $t = 1$, scaled by 0.80

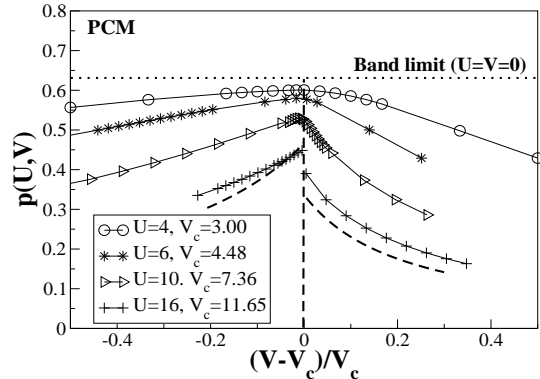


FIG. 7: Bond order $p(U, V)$ vs. $(V - V_c)/V_c$ for PCM with $U = 4, 6, 10$ and 16 . The dotted line is the band limit, $p_0 = 2/\pi$; the dashed line is the strong-coupling limit, Eq. 8 with $V_c = 11.65$ and $t = 1$, scaled by 0.75

The critical point $U^*, V^* = V_c(U^*)$ in Fig. 1 marks the BOW phase with a metallic point. The first-order transition for $U > U^*$ is between two insulating phases. One has $\rho_2 < 1/4$ and $Z > 0$, the other has $\rho_2 > 1/4$ and $Z < 0$, and there is no metallic point. In the limit of large $U = \alpha_M V_c$ (or small t), we have $p \approx 0$ according to Eq. 8. The behavior of $p(U, V)$ and its weak size dependence provides a convenient new way to find U^* . The reason is that $p(U, V)$ varies slowly with V near the maximum at $V_c(U)$, whereas $\rho_2(U, V)$ or $Z(U, V)$ vary the most rapidly there. It is then numerically easier to discern a discontinuity in $p(U, V)$.

Half-filled Hubbard models with spin-independent potentials have e-h symmetry. Their dipole allowed (one photon) and two photon excitations are consequently to different manifolds of states, as discussed extensively for linear polyenes [27]. The lowest two-photon state, 2^1A_g , has the gs symmetry and can be viewed as two triplets. Then $E_m = 0$ on the SDW side implies that the two photon gap also vanishes, while the one-photon excitation to 1^1B_u has finite energy. Conversely, finite E_m in the BOW phase implies a finite two-photon gap. While DMRG for $E(2^1A_g)$ is less accurate at present than for E_m , we find a two-photon gap of 0.138 for EHM at $U = 4, V = 2.1$, well within the BOW phase. Moreover, since the gap is much smaller than $2E_m = 0.48$, we conclude that the triplets form a bound state. A finite two-photon gap is another signature of a BOW phase.

IV. DISCUSSION

We introduced potentials $V_m(a)$ in Eq. 3 that retain the symmetry of the EHM in order to extend and widen the BOW phase sketched in Fig. 1. DMRG calculations of the magnetic gap E_m are a direct new approach to the SDW/BOW boundary. The kinetic energy or bond

order $p(U, V)$ at the metallic point turns out to be a convenient new way to evaluate the critical point U^* . Tuning the BOW phase by changing $V_m(a)$ also clarifies the electronic instability with increasing $U < U^*$ before the inevitable CDW transition at large V . The BOW phase is interesting but poorly characterized because it does not appear in the limit of either large U or large V . It is an intermediate phase with strong charge fluctuations, competition between U and V leading to magnetic frustration, and fairly large t . Translational and inversion symmetry are broken in the BOW phase, while translational and electron-hole symmetry are broken in the CDW. Finite V is required in either case.

The CDW shown in Fig. 1 is a good representation of the gs when $V \gg U$ and sites are alternately empty and doubly occupied. The SDW in Fig. 1 is a cartoon for $U \gg V$, however, since the gs of a Heisenberg antiferromagnet (HAF) is a linear combination of many states with $n_p = 1$ at all p . The Néel state shown has higher energy than the Kekulé functions, $|K1\rangle$ or $|K2\rangle$, in which adjacent spins are singlet paired, either $2p$ with $2p - 1$ or $2p$ with $2p + 1$ for all p . $|K1\rangle$ or $|K2\rangle$ is a linear combination of N -spin states, half up and half down, that includes the Néel state. The actual gs for $U \gg V$ also has singlet pairing of sites that are not adjacent.

We have deliberately omitted a BOW cartoon in Fig. 1; it is usually shown [2, 3, 4, 5] as $(\uparrow \downarrow)(\uparrow \downarrow)$ to suggest broken symmetry for bond orders. Such a representation, suitable for a dimerized HAF, is quite misleading for a BOW gs with almost 50% of empty and doubly occupied sites (Fig. 5) and large bond order (Figs. 6 and 7) for V slightly less than $V_c(U)$. Since t connects adjacent sites, large $p(U, V)$ indicates strong mixing of a singlet pair at sites $p, p+1$ and ionic singlets with $n_p = 2, n_{p+1} = 0$ or $n_p = 0, n_{p+1} = 2$. The BOW gs is a linear combination of the full Hubbard basis of 4^N states, aside from particle number or symmetry constraints. A product of dimer function $(1,2)(3,4)\dots$ gives some insight into the BOW gs. The dimer function $(1,2)$, an approximation for the BOW gs, is

$$(1, 2) = \left[\frac{\cos \theta}{\sqrt{2}} (a_{1\alpha}^\dagger a_{2\theta}^\dagger - a_{1\theta}^\dagger a_{2\alpha}^\dagger) + \frac{\sin \theta}{\sqrt{2}} (a_{1\alpha}^\dagger a_{1\theta}^\dagger + a_{2\alpha}^\dagger a_{2\theta}^\dagger) \right] |0\rangle \quad (10)$$

where $a_{p\sigma}^\dagger$ is a creation operator in Eq. 1 and θ is a variational parameter. The state in the first term is the covalent (Heitler-London) singlet; that in the second is the ionic singlet. The bond order per site is $\sin \theta \cos \theta \approx 1/2$ for equal admixture at $\theta = \pi/4$. Such $p(U, V)$ are found directly for $U < U^*$. The product function indicates a BOW with large charge fluctuations

Strong coupling gives a first-order SDW/CDW transition at $V_c = U/\alpha_M$ for $t = 0$ and no BOW phase for $U > U^*$. Corrections for finite t can readily be found. At the boundary, the energy for an electron transfer in

either the SDW or CDW gs is

$$\Delta E = U - V_c = U \left(1 - \frac{1}{\alpha_M(a)}\right) \quad (11)$$

We have $\Delta E > 0$ for $\alpha_M > 1$ and can apply perturbation theory in $t/\Delta E$. Second-order $(t/U)^2$ corrections to $E_0(U, V)/N$ on either the SDW or CDW side yield an approximate $\rho_2^{(2)}(U, V)$ according to Eq. 2. The jump at V_c decreases and vanishes at

$$U^{(2)} = \frac{2\alpha_M t \sqrt{2\ln 2 + 1}}{(\alpha_M - 1)} \quad (12)$$

$U^{(2)}$ is a simple estimate for U^* that shows how potentials with small $\alpha_M > 1$ extend the range of continuous $\rho_2(U, V)$. We obtain $U^{(2)}/t = 6.18$ for the EHM with $\alpha_M = 2$. Second order corrections yield a comparably accurate estimate for a continuous neutral-ionic transition in CT salts [28]. The values of $U^{(2)}$ are 11.1 for PCM and 16.7 for DCM. Second order corrections yield $V_c(U, a) > U/\alpha_M$ but overestimate the increase; the fourth order correction [21] for EHM reduces the increase.

Half-filled Hubbard models have spin-charge separation when $U - V$ is large compared to t . The gs on the SDW side can be mapped into an effective spin Hamiltonian for any potential V_m . Up to t^4 , H_{eff} is a HAF with $J_1, J_2 > 0$ and frustration; a magnetic gap opens [22] at $J_2/J_1 = 0.2411$. The possible connection between a BOW phase and spin frustration has been pointed out previously [21], and it is a delicate matter. Seitz and Klein [20] obtained H_{eff} up to $(t/U)^6$ for $V = 0$ in Eq. 1 by systematically considering virtual transfers in the covalent sector with $n_p = 1$ at all p ; an even number of transfers is required to end up with $n_p = 1$ at all p . Van Dongen [21] obtained H_{eff} for EHM up to $[t/(U - V)]^4$. The t^2 term gives a HAF with nearest-neighbor exchange $J_1 = 4t^2/(U - V)$, and J_1 has contributions from all higher orders. The t^4 order introduces a second-neighbor exchange J_2 , also AF, and all higher orders contribute to J_2 . Mapping into a HAF with J_1 and J_2 breaks down in the next order, even if such corrections are included in J_1 and J_2 , because t^6 generates exchange interactions among four successive spins [20]. At the t^4 level, the ratio J_2/J_1 can readily be generalized to the potentials $V_m(a)$ in Eq. 3. We obtain

$$\frac{t^2 F(a, V)}{(U - V)^2} = \frac{J_2/J_1}{1 + 4J_2/J_1} \quad (13)$$

$$F(V, a) - 1 \equiv \frac{V - V_2(a)}{U - V_2(a)} = \frac{V}{V + (a + 2)(U - V)} \quad (14)$$

The factor $F(V, a)$ reduces to $F = 1$ at $V = 0$ and to $F(V, 1) = 1 + V/U$ for the EHM. Finite E_m requires $J_2/J_1 > 0.2411$ in spin chains when the rhs of Eq. 13 is 0.1227.

Since the 1D Hubbard model is rigorously known [29] to have $E_m = 0$ for $U > 0$, $F = 1$ is insufficient to open a gap at $U/t = 2.85$ for $V = 0$ in Eq. 13. H_{eff} with J_1 and J_2 clearly fails for $(U - V) < 3t$ because it incorrectly predicts finite E_m . The EHM has $F = 1.5$ at $V = U/2$, when a magnetic gap opens at $(U - V)/t = 3.5$ according to Eq. 13 and yields $U^* = 7.0$ in surprisingly good agreement with recent calculations [4, 5] and Table 1. But the correction to J_2/J_1 goes as $[t/(U - V)]^2 \approx 8\%$ in the next order and H_{eff} has an additional term. Potentials with $a > 1$ lead to $F > 1.5$ at $V = U/\alpha_M$ and to slightly larger $(U - V)/t \approx 3.6 - 3.7$ in Eq. 13 that, however, substantially overestimates U^* in Table 1. Hence we regard the EHM result to be accidental. Growing magnetic frustration with increasing V gives insight into how a BOW phase might develop, but the actual BOW gs for $U < U^*$ and $V < V_c(U)$ has finite ρ_2 that cannot be represented by a HAF with J_1, J_2 .

We consider next the possibility of a physical realization of a BOW phase. Several obstacles were mentioned in the Introduction. The material must have quasi-1D electronic properties that can be approximated by an extended Hubbard model such as Eq. 1; it must be close to a CDW instability; and yet it must avoid the Peierls instability of half-filled bands. Electrostatic (Madelung) energies are inherently 3D. The generalization of α_M in Eq. 4 to 3D is straightforward and has been applied to CT salts [30] with neutral or ionic gs. The strong π -acceptor A = TCNQ (tetracyanoquinodimethane) forms an extensive series of salts that contain face-to-face stack of A^- ion radicals [13]. 1:1 salts correspond to a half-filled band, and 1D Hubbard-type models describe the magnetic, optical and electronic properties of TCNQ salts. Formally, Eq. 1 refers to electrons in the LUMO of TCNQ with $t \approx 0.1 - 0.3$ eV.

We recently pointed out that the A^-A^- stacks in M^+TCNQ^- salts with $M = \text{Na, K, Rb and Cs}$ are close to the CDW boundary of AA^{-2} stacks, thereby satisfying one condition for a possible BOW phase [31]. Alkali-TCNQ salts are insulators with Coulomb interactions among localized charges on M^+ and delocalized charges on A^- . Delocalization suggests that the appropriate $V_m(a)$ has $a > 0$ rather than $a = 0$ for point charges, although 3D electrostatic interactions have to be taken into account. In any case, we have *molecular* sites in Eq. 1 and the approximation of a rigid lattice with uniform spacing must extend to rigid molecules. Alkali-TCNQ salts [32] have a phase transition around $T_d \approx 300$ K to a dimerized stack whose gs is a BOW expected in systems with triplet spin excitons [13]. The A^- stacks are regular for $T > T_d$ and have inversion symmetry at each A^- . A candidate BOW phase then refers to $T > T_d$ and must have $E_m \approx k_B T_d$ in order to justify using the gs at 0 K. The molar spin susceptibility, $\chi_M(T)$, of alkali-TCNQs is small [32] ($\approx 10^{-4}$ emu) at T_d , consistent with typical Hubbard-model parameters [31]. The behavior of $\chi_M(T)$ for $T > T_d$ in these salts, however, is not consistent with a HAF, the early model of choice, or with any

Hubbard model with $E_m = 0$ and $\chi_M(0) > 0$. Finite E_m in a stack with equal spacing accounts qualitatively for $\chi_M(T)$ at $T > T_d$. But magnetic data is merely suggestive of a BOW phase.

Quasi-1D materials based on stacks of planar molecules have strong electron-vibrational coupling to molecular vibrations as well as to lattice modes. The BOW phase is an electronic instability that breaks inversion symmetry at sites. Lifting inversion symmetry has spectacular vibrational consequences that have motivated Raman and infrared studies of dimerization transitions in many systems [33], including TCNQ salts. The appearance of a totally symmetric TCNQ-vibration, polarized along the stack, in the ir spectrum at $T > T_d$ is evidence for a BOW phase. Such a mode was reported [34] for a CN stretch in K-TCNQ and rationalized in terms of dimerization fluctuations before the suggestion [2] of a BOW phase for the EHM. Several coupled modes were reported [35] in powder ir spectra at $T > T_d$ of several alkali-TCNQs. The second form of the rubidium salt, Rb-TCNQ(II), is a good candidate for a planned single crystal ir study. It has a low [32] $T_d \approx 230$ K and a crystal structure [35] with one molecule per unit cell at 300 K.

In summary, we have characterized the BOW phase of half-filled extended Hubbard models with 1D potentials $V_m(a)$ in Eq. 3. The BOW phase (Table 1) for $U < U^*$ extends from $V_s(U)$ where the magnetic gap opens to the metallic point $V_c(U)$ at the CDW boundary. The kinetic energy or gs bond order provides an accurate new estimate of the critical U^* that terminates the BOW phase. The SDW/CDW transition for $U > U^*$ is a first-order transition between two insulating phases. We find that the BOW gs has strong charge fluctuations, magnetic frustration and a finite two-photon gap. The present analysis of competing interactions is limited to electronic correlations in a 1D model. Both electron-phonon coupling and electron-molecular-vibration coupling will have to be considered to establish that several suggestive observations on alkali-TCNQ salts at $T > T_d$ can be interpreted as physical realizations of BOW systems.

Acknowledgments. ZGS thanks A. Painelli for stimulating discussions about the BOW phase of the EHM. SR thanks DST India for JC Bose National Fellowship and a grant through project no. SR/S2/CMP-24/2003. MK thanks UGC India for a senior research fellowship.

-
- [1] J.E. Hirsch, Phys. Rev. Lett. **53**, 2327 (1984); Phys. Rev. B **31**, 6022 (1985).
- [2] M. Nakamura, Phys. Rev. B **61**, 16377 (2000).
- [3] P. Sengupta, A. W. Sandvik and D.K. Campbell, Phys. Rev. B **65**, 155113 (2002).
- [4] Y.Z. Zhang, Phys. Rev. Lett. **92**, 246404 (2004).
- [5] S. Glocke, A. Klumper and J. Sirker, Phys. Rev. B **76**, 155121 (2007).
- [6] A. W. Sandvik, L. Balents and D.K. Campbell, Phys. Rev. Lett. **92**, 236401 (2004).
- [7] J. Solyom, Adv. Phys. **28**, 201 (1979).
- [8] G. P. Zhang, Phys. Rev. B **68**, 153101 (2003).
- [9] K-M Tam, S-W Tsai and D.K. Campbell, Phys. Rev. Lett. **96**, 036408 (2006).
- [10] J.W. Cannon, R.T. Scalettar and E. Fradkin, Phys. Rev. B **44**, 5995 (1991).
- [11] Z.G. Soos and S. Ramasesha, Phys. Rev. B **29** 5410 (1984).
- [12] E. Dagotto, Science, **309**, 257 (2005).
- [13] Z.G. Soos, Annu. Rev. Phys. Chem. **25**, 121 (1974); Z.G. Soos and D.J. Klein, in *Treatise on Solid State Chemistry*, Vol. III (ed. N.B. Hannay, Plenum, New York, 1976) p. 689.
- [14] A. Painelli and A. Girlando. J. Chem. Phys. **84**, 5655 (1987).
- [15] W.P. Su, J.R. Schrieffer and A.J. Heeger, Phys. Rev. Lett. **42**, 1698 (1979); Phys. Rev. B **22**, 2099 (1980).
- [16] Z.G. Soos, D. Mukhopadhyay, A. Painelli and A. Girlando, in *Handbook of Conducting Polymers*, Sec. Edit. (Eds. T.A. Skotheim, R. Elsenbaumer and T. Allen, Marcel Dekker, New York, P997) p. 165.
- [17] Y. Anusooya-Pati, Z.G. Soos and A. Painelli, Phys. Rev. B **63**, 205118 (2001).
- [18] R. Resta, Rev. Mod. Phys., **66**, 899 (1994); R. Resta, Phys. Rev. Lett. **80**, 1800 (1998).
- [19] R. Resta, J. Phys: Cond. Mat. **14**, R625 (2002); I. Souza, T. Wilkens and R.M. Martin, Phys. Rev. B **62**, 1666 (2000).
- [20] W.A. Seitz and D.J. Klein, Phys. Rev. B **9**, 2159 (1974).
- [21] P.G.J. van Dongen, Phys. Rev. B **49**, 7904 (1994).
- [22] K. Okamoto and K. Namura, Phys. Lett. A **169**, 433 (1992); R. Chitra, Swapan Pati, H. R. Krishnamurthy, Diptiman Sen, and S. Ramasesha Phys. Rev. B **52**, 6581 (1995); Manoranjan Kumar, S. Ramasesha, Diptiman Sen, Z. G. Soos, Phys. Rev. B **75**, 052404 (2007).
- [23] S. Mazumdar and D.K. Campbell, Phys. Rev. Lett. **55**, 2067 (1985).
- [24] L. Del Freo, A. Painelli and Z.G. Soos, Rev. Lett. **89**, 27402 (2002); A. Painelli and Z.G. Soos, Chem. Phys. **325**, 48 (2006).
- [25] S.R. White, Phys. Rev. B **48**, 10345 (1993)
- [26] S. Ramasesha and Z.G. Soos, in *Theoretical and Computational Chemistry*, Vol. 10, (Ed. D.L. Cooper, Elsevier, Amsterdam, 2002) p. 635.
- [27] P.C.M. McWilliams, G.W. Hayden and Z.G. Soos, Phys. Rev. B **43**, 9777 (1991).
- [28] Z.G. Soos, S. Kuwajima, and R. H. Harding, J. Chem. Phys. **85**, 601 (1986).
- [29] H. Shiba, Phys. Rev. B **6**, 930 (1972).
- [30] R.M. Metzger, in *Crystal Cohesion and Conformational Energies*, Topics in Current Phys. 26, (Ed. R.M. Metzger, Springer-Verlag, Berlin, 1981) p. 80.
- [31] M. Kumar, S. Ramasesha, R.A. Pascal, Jr. and Z.G. Soos, Euro. Phys. Lett. **83**, 37001 (2008).
- [32] J.G. Vegter and J. Kommandeur, Mol. Cryst. Liq. Cryst. **30**, 11 (1975).
- [33] R. Bozio and C. Pecile, in *Spectroscopy of Advanced Materials*, Advances in Spectroscopy, Vol. 19 (Eds. R.J.H.

- Clark and R. E. Hester, Wiley, New York, 1991) p.1.
- [34] H. Okamoto, Y. Tokura and T. Koda, Phys. Rev. B **36**, 3858 (1987).
- [35] R. Bozio and C. Pecile, J. Chem. Phys. **67**, 3864 (1977).
- [36] I. Shirotnani and H. Kobayashi, Bull. Chem. Soc. Japan **46**, 2596 (1973).